JACS
JOURNAL OF THE AMERICAN CHEMICAL SOCIETY

ARTICLE

pubs.acs.org/JACS

Chirality-Preserving Growth of Helical Filaments in the B4 Phase of Bent-Core Liquid Crystals

Dong Chen,[†] Joseph E. Maclennan,[†] Renfan Shao,[†] Dong Ki Yoon,[†,‡] Haitao Wang,[†,§] Eva Korblova,[∥] David M. Walba,[∥] Matthew A. Glaser,[†] and Noel A. Clark*[,†]

[†]Department of Physics and Liquid Crystal Materials Research Center, University of Colorado, Boulder, Colorado 80309-0390, United States

[‡]Graduate School of Nanoscience and Technology, World Class University, KAIST, Daejeon 305-701, Korea

[§]Key Laboratory of Automobile Materials (MOE) and College of Materials Science and Engineering, Jilin University, Changchun 130012, China

[∥]Department of Chemistry and Biochemistry and Liquid Crystal Materials Research Center, University of Colorado, Boulder, Colorado 80309-0215, United States

Supporting Information

ABSTRACT: The growth of helical filaments in the B4 liquid-crystal phase was investigated in mixtures of the bent-core and calamitic mesogens NOBOW and 8CB. Freezing-point depression led to nucleation of the NOBOW B4 phase directly from the isotropic phase in the mixtures, forming large left- and right-handed chiral domains that were easily observed in the microscope. We show that these domains are composed of homochiral helical filaments formed in a nucleation and growth process that starts from a nucleus of arbitrary chirality and continues with chirality-preserving growth of the filaments. A model that accounts for the observed local homochirality and phase coherence of the branched filaments is proposed. This model will help in providing a better understanding of the nature of the B4 phase and controlling its growth and morphology for applications, such as the use of the helical nanophase as a nanoheterogeneous medium.

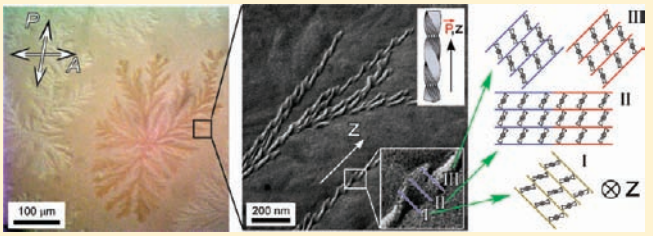

INTRODUCTION

Chirality has been one of the most attractive themes in chemistry since Pasteur's famous experiment showing the handedness of tartaric acid.[1] Understanding how chirality arises is important from the perspective of science as well as technology. In biology, for example, several models have been proposed to address the fundamental question of how enantiomerically pure solutions or crystals might have emerged from a presumably racemic prebiotic world.[2−4]

While quite common in crystals, spontaneous chirality in fluids of achiral molecules was only recently reported, with macroscopic chiral conglomerate domains observed in stacked fluid layers of banana-shaped, achiral liquid-crystal molecules. Indeed, mesogens with bent cores and one or two flexible tails exhibit a wide variety of novel structural phenomena involving the interplay of chiral, polar, and liquid-crystalline order,[5,6] including the first manifestation of ferroelectricity in a smectic phase of achiral molecules.[7] The strong local preference for layering, coupled with the bent shape of the molecules, leads to two spontaneous, symmetry-breaking instabilities: polar molecular orientational ordering and molecular tilt.[8] These instabilities combine to drive the formation of chiral layered phases such as the B2 and B7 phases.[9,10]

It has recently been shown that in both the dark conglomerate and B4 phases of banana-shaped molecules there is a preference for the smectic layers to have saddle-splay curvature.[11,12] This tendency is attributed to the orthogonal tilt directions of the two molecular half-arms, which cause dilation in one half-layer and compression in the other. This produces a frustrated state that can be relieved by saddle-splay curvature, a response that accommodates both the chirality and the layering. While the dark conglomerate phase is composed of disordered focal conic domains, the B4 phase forms helical nanofilaments. Even though 1,3-phenylenebis[4-(4-octoxyphenyliminonetyl)benzoate] (NOBOW) is an achiral molecule, in a mechanism common to many bent-core phases, spontaneous symmetry breaking causes the B4 phase to be chiral. To date, however, the B4 phase is unique in being the only bent-core phase with a macroscopically chiral structure, the twisted filament [for a discussion of the hierarchical self-assembly of the nanofilament phase, see the Supporting Information (SI)]. The macroscopic chirality of the dark conglomerate phase is maintained by the local chiral organization of the molecules and the long-range continuity of

Received: April 17, 2011
Published: June 21, 2011

the smectic layers. However, the establishment of macroscopic chirality in the B4 phase, which is composed of distinct left- or right-handed helical filaments, has remained a mystery.

In this work, we investigated mixtures of the bent-core mesogen NOBOW and the calamitic liquid crystal 4-*n*-octyl-4′-cyanobiphenyl (8CB) in order to explore the origin of macroscopic chirality in the NOBOW B4 phase. The observation of unusually large chiral domains (of millimeter dimensions) in depolarized transmission light microscopy (DTLM) of mixtures of the rod-shaped mesogen 4-*n*-pentyl-4′-cyanobiphenyl (5CB) or 8CB with NOBOW led to their being intensively investigated.[13−16] The 8CB/NOBOW system can be well-understood in terms of "nanoscale phase separation", with the 8CB filling the volume between dilute, random networks of NOBOW B4 helical filaments. NMR measurements showed that 8CB is prealigned far above the bulk 8CB Iso−N transition, forming a thin, ordered sheath around the B4 filaments.[16] The nanosegregation of 8CB was confirmed by freeze-fracture transmission electron microscopy (FFTEM) images obtained with 8CB in the nematic phase and X-ray scattering experiments with 8CB in the smectic-A phase.[15]

The mixtures provide a good platform for investigating the development of chirality in the B4 phase, as in neat NOBOW the B4 phase grows in from the B2 phase, making it difficult to distinguish the nucleation events. In the mixtures, the B4 phase appears directly from the isotropic phase, forming large chiral domains in which the growth of the phase can be directly observed. In addition, because of the dilution with 8CB, each chiral domain comprises a network of individual B4 filaments, allowing visualization of how new helical nanofilaments branch off from existing ones.[13] More importantly, phase segregation combined with spontaneous nanoscale self-assembly of the B4 helical nanofilaments offers the possibility for a wide variety of novel materials. Understanding the nucleation and growth behavior of the B4 helical nanofilament in the blends will help in their application, such as their use as nanoheterogeneous media.

RESULTS AND DISCUSSION

The chemical structure and phase behavior of 8CB/NOBOW mixtures shown in Figure 1a have been reported previously.[15,16] The chirality of the mixtures was investigated by combining DTLM, which reveals the macroscopic texture and optical activity, with FFTEM, which shows the chirality of individual nanofilaments. For DTLM, 4 μm thick cells with rubbed polyimide alignment layers were filled with isotropic liquid crystal through capillary force. In pure NOBOW samples, the B4 phase comes in below the B2 phase and shows a uniform bluish color under crossed polarizers, with the texture resolved into left- and right-handed chiral domains when the polarizers are decrossed.[12] In mixtures with an 8CB concentration (c) above 25% (expressed in wt %), the B4 phase appears directly from the isotropic melt at temperatures far above the clearing point of 8CB. When the B4 phase first appears, large homochiral domains with sizes of several millimeters and random handedness grow out from distinct nuclei until they fill the available volume in the cell. For an 8CB/NOBOW mixture with c = 50%, conventional optical activity is observed in the B4 phase. The sample is dark when viewed between crossed polarizers because of its low birefringence, while uncrossing the polarizers by 5° reveals that each nucleation domain has a random but well-defined handedness that is maintained as it

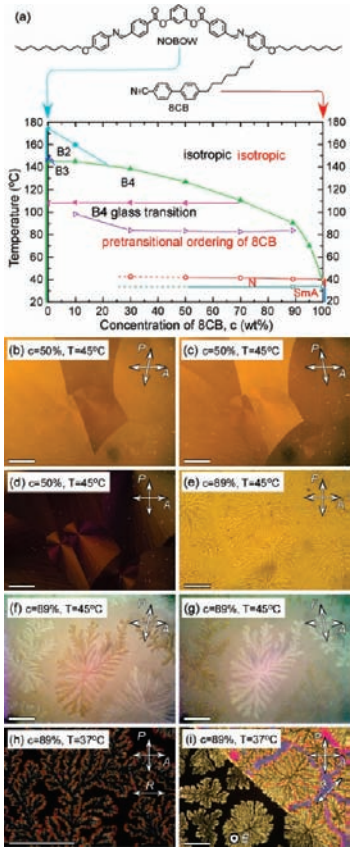

Figure 1. Phase diagram and DTLM images of 8CB/NOBOW mixtures in 4 μm thick planar-aligned cells. (a) Structures of NOBOW and 8CB and a phase diagram for the binary system derived from differential scanning calorimetry (DSC) and DTLM observations (for a simplified phase diagram, see the SI). Mixtures of NOBOW and 8CB form a single, homogeneous phase only in the high-temperature, isotropic range. At lower temperatures, the NOBOW B4 phase separates into a network of helical nanofilaments, leaving 8CB to fill the interstitial spaces (NOBOW phases are shown in black and 8CB phases in red). The decrease in the NOBOW Iso−B4 transition temperature with increasing 8CB concentration (c) corresponds to conventional freezing-point depression. (b−d) DTLM images of a c = 50% 8CB/NOBOW mixture at 45 °C, where 8CB is isotropic and NOBOW is in the B4 phase: (b) Left- and (c) right-handed chiral domains can be observed when the polarizers are decrossed. The sample is dark between the crossed polarizer and analyzer, with negligible birefringence under regular illumination. (d) With much stronger illumination, we see that each chiral region comprises a single domain with a radial orientation of the local optic axis. (e−i) DTLM images of a c = 89% 8CB/NOBOW mixture at different temperatures: (e) Dendritic domains of the B4 phase can be distinguished from the interspersed isotropic 8CB medium (T = 45 °C) as a result of an index mismatch at their interface. (f, g) The dendritic domains are chiral, as evidenced by their opposite optical activities revealed with decrossed polarizers. (h) When 8CB undergoes the Iso−N transition (T = 37 °C), 8CB is locally aligned by the NOBOW B4 dendrites, with the alignment extending ~2 μm from the B4 boundaries, giving them a thin magenta outline. The details of this alignment are still under investigation. Far from the NOBOW dendrites, 8CB is planar-aligned by the glass surface. (i) In an applied electric field of 10 V/μm (lower left half of the image), 8CB aligns with the field, giving homeotropic orientation and optical extinction, while the dendritic B4 regions do not respond. All scale bars represent 100 μm, and the double-headed arrows indicate the planar alignment direction. The contrast in (b), (c), (e), (f), and (g) was enhanced using Adobe Photoshop.

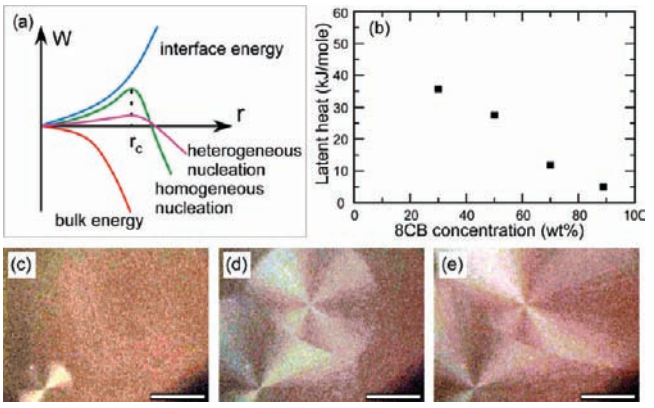

Figure 2. Energetics and real-time observation of chiral domain nucleation and growth of the NOBOW B4 phase in 8CB/NOBOW mixtures. (a) Competition between the energy gained by creating a new volume of B4 ($-{}^4/_3\pi r^3 G_v$, red curve) and the cost of surface tension ($4\pi r^2\gamma$, blue curve) results in a finite energy barrier to homogeneous nucleation (green curve) and a critical radius r_c. For heterogeneous nucleation, such as in the case of chiral doping, r_c is the same as for homogeneous nucleation, but the energy barrier of domains with the same chirality as the dopant is reduced (magenta curve). (b) The normalized latent heat of the NOBOW Iso−B4 phase transition decreases as the concentration of NOBOW decreases. (c−e) DTLM images showing the nucleation and growth of B4 domains in a c = 50% 8CB/NOBOW mixture in a 4 μm cell at 128 °C at 1 s intervals. All scale bars represent 100 μm, and the growth velocity is ∼0.1 μm/ms. The contrast has been enhanced using Adobe Photoshop.

grows. Eventually the cell becomes filled with distinct left- and right-handed chiral domains, distinguished by their opposite optical activities (Figure 1b,c). When the illumination is very strong, we can see using crossed polarizers that each region with uniform chirality comprises a single domain with a pattern of birefringence corresponding to a local optic axis pointing radially outward from the nucleation center (Figure 1d). This birefringence reflects anisotropy in the B4 filament organization as the phase grows out from the nucleation site. At high NOBOW concentrations (e.g., c_{NOBOW} = 50 wt %), the B4 phase grows in as domains with smooth circular boundaries, which eventually become parabolic when different domains meet. As the NOBOW concentration is decreased, the B4 phase growth morphology changes from circular to fractal domains. In mixtures with low NOBOW concentrations (e.g., c_{NOBOW} = 11 wt %), a fantastic dendritic texture is observed when the B4 phase nucleates and grows within the isotropic 8CB medium (Figure 1e), with the chirality of the phase revealed by its optical activity (Figure 1f,g). When the sample is subsequently cooled so the 8CB undergoes the isotropic-to-nematic (Iso−N) transition, the 8CB in the vicinity of the NOBOW dendrites becomes aligned by the B4 filaments (Figure 1h), while further from the NOBOW domains, the 8CB is planar-aligned by the glass surface. A sufficiently strong applied electric field causes the 8CB component to orient along the field direction, while the NOBOW shows no response (Figure 1i, bottom left). These optical observations all confirm that the chiral NOBOW domains grow from distinct nucleation sites and that the chirality is maintained as the domains grow.

In the absence of preferred nucleation sites, B4 domains are expected to nucleate homogeneously. If we assume that each domain starts as a spherical cluster of radius r that liberates a latent heat $-G_v$ (energy/volume) during formation but must pay the cost γ (energy/area) of creating the surface that interfaces with the surrounding isotropic material, then the change in free energy in forming such a cluster is $W = -{}^4/_3\pi r^3 G_v + 4\pi r^2\gamma$. These bulk and interfacial energies are sketched in Figure 2a, where we see that below a critical radius $r_c = 2\gamma/G_v$, adding molecules to the B4 cluster costs free energy (green curve in Figure 2a). We expect the surface tension γ at the interface to depend on such properties of the B4 filaments as the smectic layer spacing d, the filament width w, and the helix pitch p. The smectic layer spacing in the B4 filaments is independent of the 8CB concentration,[15] and the helix pitch and width are also invariant (Table 1). It therefore seems reasonable to assume that γ stays the same over the whole concentration range. However, the magnitude of the normalized latent heat of the I−B4 transition, which is essentially equivalent to G_v, decreases significantly as the NOBOW concentration decreases (Figure 2b). This implies that the critical radius for nucleation of the B4 phase increases as the NOBOW is progressively diluted. Since the Iso−B4 phase transition occurs at temperatures above 100 °C in the mixtures, NOBOW molecules undergo rapid diffusion in the isotropic phase and are able to reach the site of nucleation quickly enough to promote growth. In this scenario, the nucleation rate is limited by the average number of critical clusters, while the critical radius r_c is enhanced in the mixtures, so only a very few nuclei can reach the critical radius r_c, aided for example by thermal fluctuations or supercooling. Another factor that may also contribute to the formation of large chiral domains in the mixtures is that the increased coexistence range of the Iso and B4 phases in the mixtures leads to a reduction in the effective cooling rate. In practice, it is much easier to get large homochiral domains in the mixtures than in pure NOBOW. Figure 2c−e shows an example of domain nucleation and growth for a c = 50% 8CB/NOBOW mixture.

Table 1. Helical B4 Filament Characteristics in 8CB/NOBOW Mixtures[a]

8CB concentration (%)	0	30	50	75	95
helix pitch p (nm)	217 ± 6	221 ± 4	218 ± 6	217 ± 3	216 ± 6
filament width w (nm)	37 ± 2	37 ± 3	37 ± 2	36 ± 3	38 ± 8

[a] The helix pitch p and filament width w were measured as functions of composition (% 8CB) from FFTEM images, as indicated in Figure 3a. The reported uncertainties are standard deviations obtained from five measurements on each mixture. The helix structure shows little dependence on the 8CB concentration.

The degeneracy of left- and right-handed chiral domains of a liquid-crystal phase can be lifted in a variety of ways.[8,17−22] For example, an imbalance of chirality can be produced by an external chiral stimulus, such as weak chiral doping to give strong "sergeants-and-soldiers" enantioselection of B4 chirality,[8,17] chiral surface treatments with polyimide layers possessing chiral side chains,[18] growth from a twisted nematic[19] or chiral B2 phase,[20] illumination with circularly polarized light,[21] or the use of a nonchiral polymer network template to achieve a macroscopically chiral structure.[22] These effects can be understood in the general context of heterogeneous nucleation theory. For example, in the case of chiral doping, the critical radius for nucleation remains unchanged while the energy barrier that must be overcome for heterogeneous nucleation of domains of the same chirality as the dopant is greatly reduced, facilitating nucleation (magenta curve, Figure 2a).

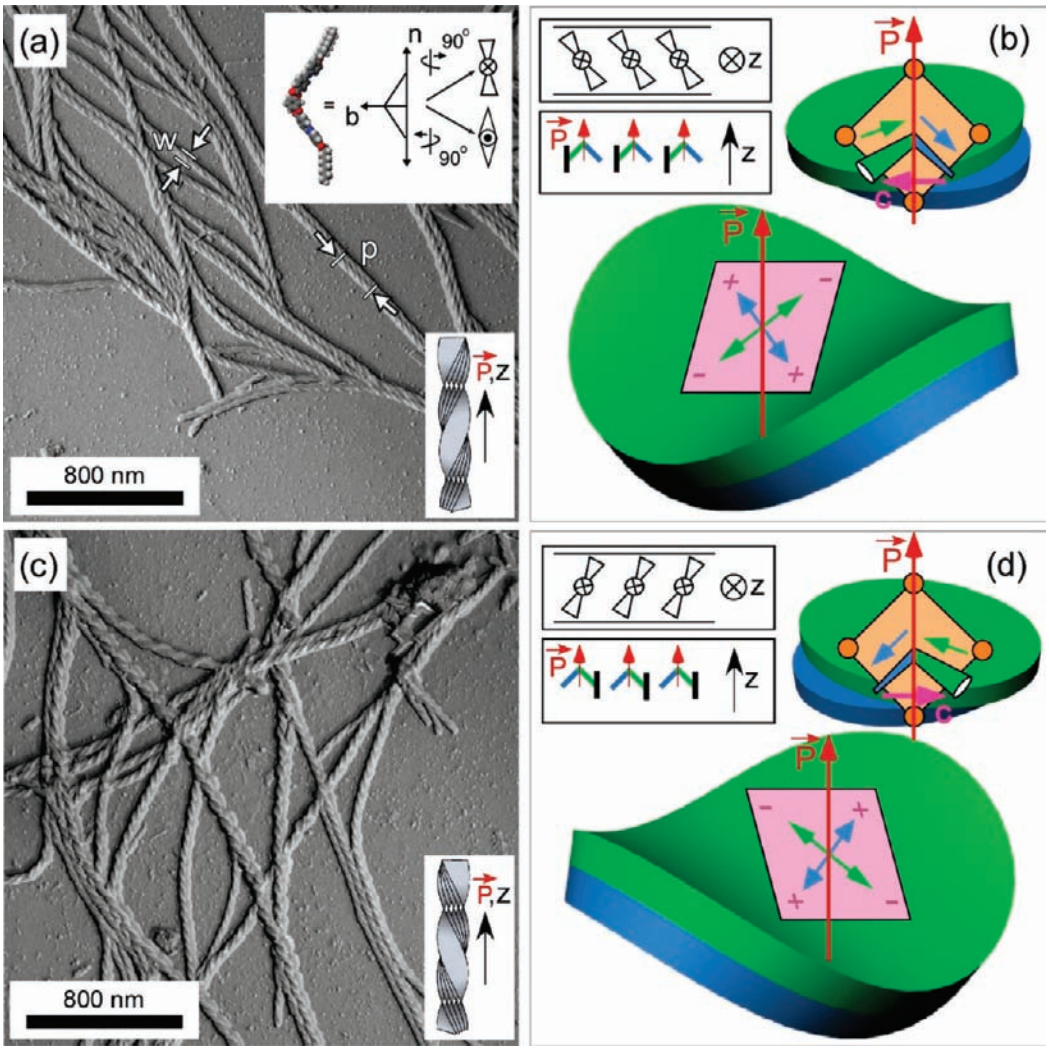

Figure 3. Left- and right-handed B4 filaments and their corresponding molecular organization. FFTEM images of a c = 75% 8CB/NOBOW mixture quenched at 37 °C reveal large homochiral regions with either (a) left- or (c) right-handed helices. Such images suggest that the macroscopic chiral domains of the B4 phase seen in the optical microscope comprise exclusively left- or right-handed helical filaments. The inset in (a) shows the convention for the molecular director **n** and the molecular bow direction **b** of bent-core molecules, with the polarization **P** along **b**. The handedness of the helices is determined by the corresponding layer chirality, as shown in (b) and (d). Each molecular arm can be viewed as an elastically isotropic slab that dilates parallel to and compresses perpendicular to the molecular tilt direction as a result of the hexagonal in-plane ordering.[11,12] Because the tilt directions of the top and bottom molecular arms are orthogonal, the two elastic slabs adopt a saddle-splay curvature to relieve the intralayer mismatch. The local layer chirality, which is determined by the polarization and molecular tilt, results in distinct regions with orthogonal saddle-splay and opposite signs of filament twist. The filament widths w and helix pitches p measured for different mixtures are shown in Table 1.

FFTEM, which enables visualization of structure on nanometer length scales, revealed many details of the local layer organization in the B4 phase. Our observations of 8CB/NOBOW mixtures confirmed that the B4 phase is made of individual helical filaments[12] and showed unambiguously that these occur with both left- and right-handed twists, as illustrated in Figure 3a,c. We propose that the handedness of the B4 helices determines the global chirality of the macroscopic homochiral domains observed by DTLM, such as those shown in Figure 1, with homochiral filaments organizing collectively into locally ordered arrays of coherent twist that extend over visible length scales to form macroscopic chiral domains. In many hundreds of B4 FFTEM images of a variety of samples, a consistent feature of the B4 filaments is that they are of the same handedness over large areas. No mixing of left- and right-handed helical filaments was ever observed, even in images covering many square micrometers. This is consistent with the optical observation that the B4 domains are large and homochiral and have distinct boundaries, as shown in Figure 1. The twist sense of the helical filaments depends on the layer chirality of the tilted, polar bent-core molecules, as sketched in Figure 3b,d (for general arguments concerning molecular tilt, polarity and chirality, see the SI). Because of the in-plane hexagonal ordering of the molecules,[12] the molecular arms dilate along the tilt direction, with the top and bottom arms (modeled as elastic slabs at the top right in Figure 3b,d) tilting in orthogonal directions. In order to relieve the stress induced by the mismatch of the top and bottom core arms of the banana molecules, saddle-splay curvature of the layers is adopted. When this is coupled with the polarization of the phase (the saddle-splay curvature itself is achiral), the structure is chiral and favors one sign of helical twist of the nanofilament, either left-handed (Figure 3b) or right-handed (Figure 3d). In other words, the

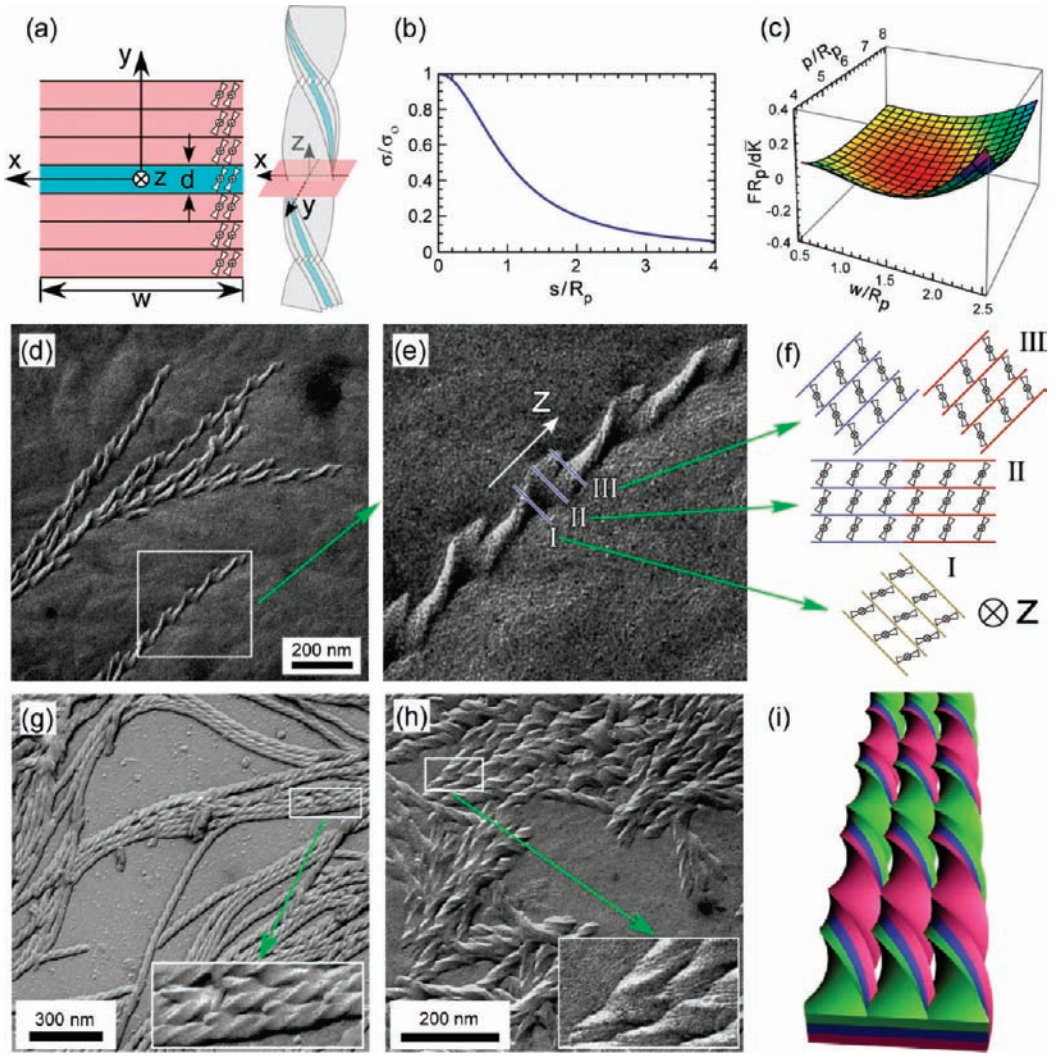

Figure 4. Chirality-preserving growth of helical B4 filaments. (a) Cross section (pink plane) of a helical filament, showing the filament width along x, thickness along y, and length along z. The molecules are tilted, with the polarization oriented along z, the helix axis. d is the smectic layer spacing. (b) Normalized principal curvature of the central layer of the filament [shaded blue in (a)] as a function of the normalized distance from the helix axis, assuming that the principal curvature σ is equal to the preferred curvature σ_o at $s = 0$. The normalization constant R_p is equal to $1/\sigma_o$. Away from the helix axis, the layers deviate from the ideal shape, at the cost of higher elastic energy. (c) Normalized energy gained per unit length of filament central layer as a function of scaled filament width and helix pitch, as given by eq 1. Minimization of the energy assuming $G_v R_p^2/\bar{K} = 0.1$ gives a maximum reduced filament width $w_{max}/R_p \approx 1.43$ and a reduced helix pitch $p/R_p \approx 5.57$. For $w > w_{max}$ in this model, the reduction of the Gibbs energy achieved by widening of the filament cannot compensate for the associated increase in the elastic energy. (d) FFTEM image showing chirality-preserving dendritic growth of helical filaments. New filaments branch from the center of an existing one to form a pair of filaments with the same twist. The region in the white box is enlarged in (e) to show the helix branching more clearly. (f) Cross sections of the helical filament near the branching area as marked in (e). Since the molecular organization is preserved during widening, both the chirality and the twist of the branched filaments are the same as those of the original one, and neighboring helices are naturally phase coherent. (g) FFTEM image of a $c = 75\%$ 8CB/NOBOW mixture showing the remanents of neighboring filaments above, most of which have been removed by fracture (magnified in the inset). (h) FFTEM image of pure NOBOW showing filament branching. The inset shows the layer edges and surfaces in a branching region. (i) Model of a bundle of homochiral, phase-coherent, helical B4 nanofilaments.

twist of the filaments (structural chirality) is a consequence of the local layer chirality resulting from the interplay of molecular polarization and tilt.

The unusual size of the homochiral domains and our ability to make direct observations of domain growth in the mixtures prompted us to speculate about a mechanism of filament growth in which their handedness is preserved. If each filament nucleates and grows individually from the isotropic phase, random mixtures of left- and right-handed filaments would be expected. Since the filaments are all left-handed or all right-handed over large areas, the nucleation and growth process is chirality-preserving, with the chirality of new filaments determined by that of the filaments already present. We propose that the helicity in each domain is preserved through a growth process that starts from a single nucleus rather than forming each filament individually with a random handedness. In general, an isotropic NOBOW molecule can either attach to the ends of an existing B4 filament to make it longer, attach to the side of the filament to make it wider, or form a new layer on the filament surface. However, X-ray reflections from the B4 smectic layers showed diffuse peaks,

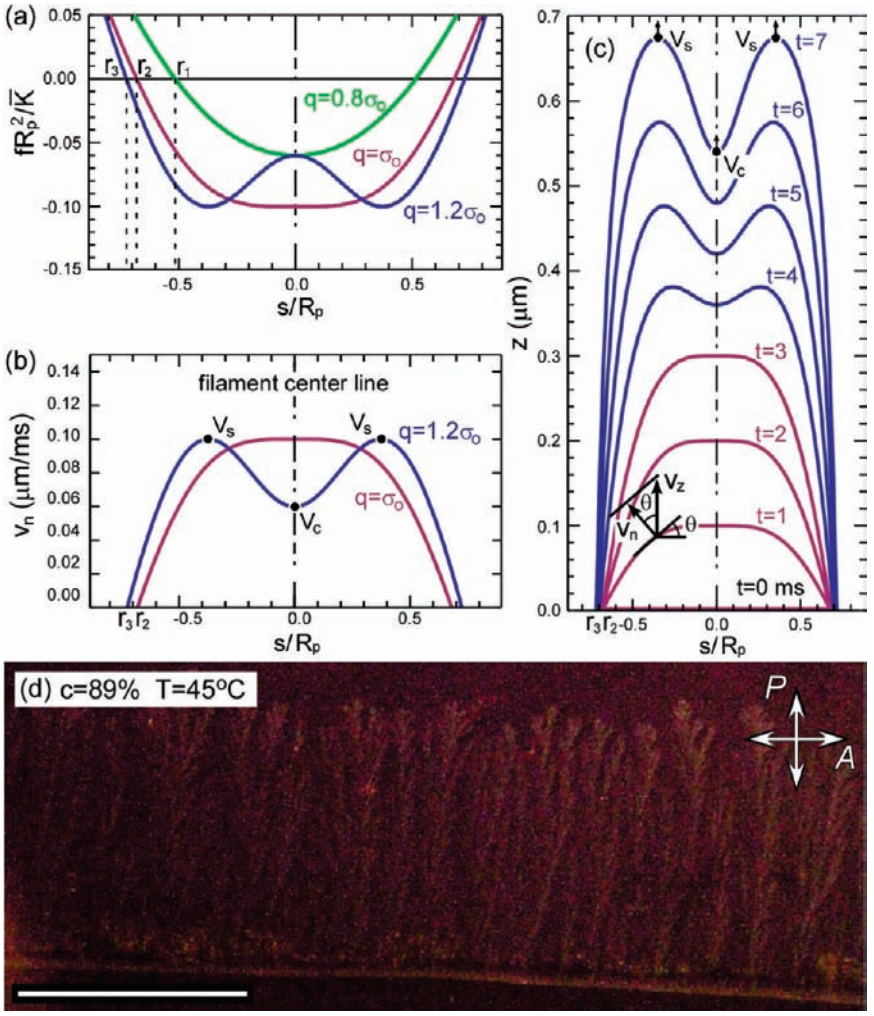

Figure 5. Kinetic analysis of filament tip growth. (a) Normalized energy density gained during growth as a function of normalized distance from the helical axis for different values of q, as labeled in the plot. When the helical twist pitch ($p = 2\pi/q$) is large (i.e., $q < \sigma_o$), growth occurs fastest along the helix axis ($s = 0$). For p less than a critical twist pitch $p_{crit} = 2\pi/\sigma_o$ (i.e., for $q > \sigma_o$), however, more energy is released per unit volume by growth of the off-axis "shoulders" of the filament tips, and these regions therefore grow faster. The corresponding final filament radii r are indicated at the left. (b) Velocity profile v_n as a function of normalized distance from the helix axis for $q = \sigma_o$ and $q = 1.2\sigma_o$. (c) Analytic simulation of filament tip growth starting from a planar growth front, first using the velocity profile assuming $q = \sigma_o$ (magenta curves) and then the profile for $q = 1.2\sigma_o$ (blue curves), which leads to tip bifurcation. (d) Heterogeneous nucleation and directional growth of helical filaments at the edge of a cell (bottom of image) to give macroscopically aligned helical nanofilaments. The scale bar represents 50 μm.

which indicate layer correlations over distances of only 40 nm, implying that the nanofilament thickness is limited to about eight smectic layers. Although the layers show only short-range order, they are robust, giving several harmonics in the X-ray reflection pattern.[12] Thus, we first focus on growth that makes the filaments wider, arguing that the final filament width is determined by the elastic energy of the layers.

As we have mentioned previously, saddle-splay curvature is adopted in order to relieve the stress induced by the mismatch of the top and bottom core arms of the banana molecules,[11,12] which leads to a preferred saddle-splay curvature value. For a minimal surface such as a B4 helical filament, the elastic energy cost is given by $f_E^m = \overline{K}(\sigma - \sigma_o)^2$, where $\overline{K}$ is the Frank elastic constant for Gaussian curvature and $\sigma_o = 1/R_p = G/\overline{K}$ gives the preferred curvature (for the derivation of the elastic energy density, see the SI).[12] However, in a thermotropic smectic phase, where the layers are constrained to have constant spacing, the preferred saddle-splay arrangement cannot be maintained over long distances, and the principal curvature σ of the central layer of the filament (Figure 4a) varies as $\sigma = q/(1 + q^2s^2)$, where $p = 2\pi/q$ is the helix pitch and s is the displacement from the helix axis (for the derivation of the principal curvature of the filament central layer, see the SI).[23,24] Figure 4b shows how the curvature decreases toward the outside of a helical filament having the preferred curvature σ_o at $s = 0$. As the sample is cooled into the B4 range, the ribbon can lower its free energy by gaining the Gibbs energy G_v, releasing latent heat. The energy density gained during growth can be expressed as $f = f_E^m - G_v$, so the energy gained per unit length of a filament central layer having width w and thickness d is given by

$$F = \int_V (f_E^m - G_v)\, dV$$

$$= \overline{K}d \int_{-w/2}^{w/2} [(\frac{q}{1 + q^2s^2} - \sigma_o)^2 - \frac{G_v}{\overline{K}}] \sqrt{1 + q^2s^2}\, ds \qquad (1)$$

dx.doi.org/10.1021/ja203522x |J. Am. Chem. Soc. 2011, 133, 12656–12663

where we have neglected the surface tension term ($\propto r^2$) because it is small in comparison with the bulk terms ($\propto r^3$) in the growth process (for the derivation of eq 1, see the SI). This normalized linear energy density is plotted in Figure 4c as a function of scaled filament pitch and width. Analytical minimization using Mathematica yielded $w_{max}/R_p \approx 1.4$ and $p/R_p \approx 5.6$ when $G_vR_p^2/\bar{K} = 0.1$. For $p = 217$ nm (a typical helix pitch observed in the FFTEM images), we predict a preferred maximum filament width (w_{max}) of 54 nm, which is similar to what is observed experimentally (confirming that $G_vR_p^2/\bar{K} = 0.1$ is a good estimate of the dimensionless constant, which will be used again in the energy density argument below). In our model, the high elastic energy cost makes the growth of filaments beyond w_{max} unfavorable. We propose that for this reason, the filaments eventually split, lowering the overall elastic energy while continuing to gain Gibbs energy as more material is added to the filaments. Examples of such filament bifurcation are shown in the FFTEM images in Figures 4d,e; a cross-section of the bifurcating filament is sketched in Figure 4f. The layer chirality is preserved as the filament grows wider. When the filament branches into two filaments, the two new filaments twist in phase with each other. Further examples of branching are shown in Figure 4g,h, while Figure 4i depicts an array of collectively organized filaments in this filament growth scenario.

The preceding analysis is based on minimizing the total free energy per unit length of the central layer of the filament. We now extend these arguments by considering the kinetics of filament growth to show that local variations in the elastic energy determine the growth velocity profile of the filament tip and lead to spontaneous bifurcation. As discussed above, the energy density gained during filament growth is given by

$$f = f_E^m - G_v = \bar{K}\sigma_o^2\left[\left(\frac{q/\sigma_o}{1 + (q/\sigma_o)^2(s/R_p)^2} - 1\right)^2 - \frac{G_vR_p^2}{\bar{K}}\right] \quad (2)$$

(for the derivation of eq 2, see the SI). Figure 5a shows the normalized energy density as a function of normalized distance from the helix axis for three different helix pitches and the corresponding preferred final filament radii, assuming $G_vR_p^2/\bar{K} = 0.1$. In all cases, $f < 0$ for small s/R_p, favoring growth when the filaments are thin, and $f > 0$ for large s/R_p, where the elastic energy cost is larger than the Gibbs energy gained, causing the growth to terminate and giving the final radius of the filament. The final filament radius (r_1, r_2, r_3) increases with q, indicating that filaments that twist more tightly can gain more free energy by increasing their width. Since the growth velocity normal to the Iso−B4 interface, $v_n(s)$, is linearly proportional to the energy density gained (the energetic driving force) and is thus a function of the radial displacement s: $v_n = 0$ when $f > 0$, and when $f < 0$, the velocity profile is of the form

$$v_n(s/R_p) \propto |f_E^m - G_v| \propto 0.1 - \left(\frac{q/\sigma_o}{1 + (q/\sigma_o)^2(s/R_p)^2} - 1\right)^2 \quad (3)$$

To obtain the values of v_n in Figure 5b, we chose the constant of proportionality in eq 3 (not shown) to be 1 μm/ms in order to match typical experimental velocities, which are ~0.1 μm/ms. Figure 5b shows the velocity profiles for $q = \sigma_o$ and $q = 1.2\sigma_o$. In order to illustrate how the velocity field leads to bifurcation of the filament tip, we computed the advance of the tip in time using the expression $z(t + \Delta t) = (v_n/\cos\theta)\Delta t + z(t)$, where θ is the inclination of the filament tip (Figure 5c), starting from a plane front. When $q = \sigma_o$, the steady-state tip is parabolic in shape, and the tip has a constant growth velocity $v_n(s/R_p = 0)$ (magenta curves in Figure 5c). When $q > \sigma_o$, the growth velocity along z at the two sides ("shoulders") of the filament, v_s, is much larger than that at the filament center line, v_c (see Figure 5b,c), and the two sides of the filament grow much faster than the center, eventually causing the tip to bifurcate (blue curves in Figure 5c). This result is consistent with the experimental observations that the tip front is parabolic and the filaments always bifurcate symmetrically about the center.

From the above discussion, we know that NOBOW B4 helical nanofilaments in the mixtures are quite robust, expelling 8CB and forming nanofilaments identical to those seen in pure NOBOW, which means that in the NOBOW/8CB system, the NOBOW B4 phase is totally phase-separated from the 8CB on the molecular scale. On the other hand, through the bifurcation of growing filaments, the B4 phase forms a random network of homochiral filaments. At low 8CB concentration (below c = 50%), 8CB is microscopically (tens of nm in scale) homogeneously mixed with this random network,[15,25] and no bulk 8CB is observed in this regime. Such phase segregation on the molecular scale combined with mixing on the microscopic scale makes the system ideal for the development of a wide variety of novel materials. For example, the chiral boundary condition presented by the B4 helical nanofilaments enables nematic 5CB (an achiral rod-like molecule) to fill space with a chiral director field, which strongly enhances the nonlinear optical rotation.[14]

The B4 phase is one of the most complex hierarchical self-assemblies known in soft materials. We have directly observed and characterized chirality-preserving growth of the B4 helical nanofilaments in NOBOW/8CB mixtures. The alignment of bent-core liquid-crystal phases in general has been a challenging and interesting topic, and understanding the nucleation and growth behavior of the helical nanofilaments in the B4 phase suggests novel ways of achieving macroscopic alignment of those nanofilaments. As shown in Figure S.4 in the SI, the B4 phase shows birefringence in the depolarized transmission light microscope when the sample is sheared in the B2 phase.[26] FFTEM images of sheared B4 cells unambiguously show that the nanofilaments are macroscopically aligned, which accounts for the anisotropic optical index observed by DTLM. The helical nanofilaments can also be aligned effectively over large areas along one global direction by heterogeneous nucleation, for example using directional growth at the edge of a cell, as shown in Figure 5d.

CONCLUSION

Freeze-fracture transmission electron microscopy images have confirmed that the B4 helical filaments of NOBOW observed in mixtures with 8CB, a calamitic mesogen that is not soluble in the B4 phase, are structurally identical to those seen in pure NOBOW. Addition of 8CB results in the formation of large homochiral domains, allowing the nucleation and growth of individual B4 chiral domains to be characterized. The constraint of constant smectic layer spacing in the B4 banana phase prevents the establishment of globally uniform saddle-splay curvature in the twisted filaments, with the local curvature of the smectic layers deviating from the preferred value as the distance from the

helix axis increases. In order to lower the Gibbs free energy by continued growth without accumulating excess elastic energy, filaments that reach a certain width exhibit spontaneous branching. As each filament has a specific layer chirality, an existing filament and all of its branches are naturally homochiral, with the layers of adjacent filaments twisting in phase. The kind of spontaneous nanoscale self-assembly of the B4 helical nanofilaments offers the possibility for the development of a wide variety of novel materials.

■ ASSOCIATED CONTENT

Supporting Information. Complete refs 10 and 12; hierarchical self-assembly of the nanofilament phase; general arguments concerning molecular tilt, polarity, and chirality; a simplified phase diagram; derivation of the elastic energy density, the principal curvature of the filament central layer, and eqs 1 and 2; and B4 filament alignment by shearing. This material is available free of charge via the Internet at http://pubs.acs.org.

■ AUTHOR INFORMATION

Corresponding Author
Noel.Clark@colorado.edu

■ ACKNOWLEDGMENT

We thank Gareth P. Alexander for beneficial discussions. This work was supported by NSF MRSEC Grant DMR-0820579 and NSF Grant DMR-0606528.

■ REFERENCES

(1) Pasteur, L. *Ann. Chim. Phys.* **1848**, *24*, 442.
(2) Kondepudi, D. K.; Kaufman, R. J.; Singh, N. *Science* **1990**, *250*, 975.
(3) McBride, J. M.; Tully, J. C. *Nature* **2008**, *452*, 161.
(4) Noorduin, W. L.; Izumi, T.; Millemaggi, A.; Leeman, M.; Meekes, H.; Van Enckevort, W. J. P.; Kellogg, R. M.; Kaptein, B.; Vlieg, E.; Blackmond, D. G. *J. Am. Chem. Soc.* **2008**, *130*, 1158.
(5) Takezoe, H.; Takanishi, Y. *Jpn. J. Appl. Phys.* **2006**, *45*, 597.
(6) Reddy, R. A.; Tschierske, C. *J. Mater. Chem.* **2006**, *16*, 907.
(7) Niori, T.; Sekine, T.; Watanabe, J.; Furukawa, T.; Takezoe, H. *J. Mater. Chem.* **1996**, *6*, 1231.
(8) Link, D. R.; Natale, G.; Shao, R.; Maclennan, J. E.; Clark, N. A.; Körblova, E.; Walba, D. M. *Science* **1997**, *278*, 1924.
(9) Walba, D. M.; Körblova, E.; Shao, R.; Maclennan, J. E.; Link, D. R.; Glaser, M. A.; Clark, N. A. *Science* **2000**, *288*, 2181.
(10) Coleman, D. A; et al. *Science* **2003**, *301*, 1204.
(11) Hough, L. E.; Spannuth, M.; Nakata, M.; Coleman, D. A.; Jones, C. D.; Dantlgraber, G.; Tschierske, C.; Watanabe, J.; Körblova, E.; Walba, D. M.; Maclennan, J. E.; Glaser, M. A.; Clark, N. A. *Science* **2009**, *325*, 452.
(12) Hough, L. E.; et al. *Science* **2009**, *325*, 456.
(13) Takanishi, Y.; Shin, G. J.; Jung, J. C.; Choi, S.-W.; Ishikawa, K.; Watanabe, J.; Takezoe, H.; Toledano, P. *J. Mater. Chem.* **2005**, *15*, 4020.
(14) Otani, T.; Araoka, F.; Ishikawa, K.; Takezoe, H. *J. Am. Chem. Soc.* **2009**, *131*, 12368.
(15) Zhu, C.; Chen, D.; Shen, Y.; Jones, C. D.; Glaser, M. A.; Maclennan, J. E.; Clark, N. A. *Phys. Rev. E* **2010**, *81*, No. 011704.
(16) Chen, D.; Zhu, C.; Shoemaker, R.; Korblova, E.; Walba, D. M.; Glaser, M. A.; Maclennan, J. E.; Clark, N. A. *Langmuir* **2010**, *26*, 15541.
(17) Araoka, F.; Takanishi, Y.; Takezoe, H.; Kim, A.; Park, B.; Wu, J. W. *J. Opt. Soc. Am. B* **2003**, *20*, 314.
(18) Shiromo, K.; Sahade, D. A.; Oda, T.; Nihira, T.; Takanishi, Y.; Ishikawa, K.; Takezoe, H. *Angew. Chem., Int. Ed.* **2005**, *44*, 1948.
(19) Choi, S.-W.; Kang, S.; Takanishi, Y.; Ishikawa, K.; Watanabe, J.; Takezoe, H. *Angew. Chem., Int. Ed.* **2006**, *45*, 6503.
(20) Niwano, H.; Nakata, M.; Thisayukta, J.; Link, D. R.; Takezoe, H.; Watanabe, J. *J. Phys. Chem. B* **2004**, *108*, 14889.
(21) Choi, S.-W.; Izumi, T.; Hoshino, Y.; Takanishi, Y.; Ishikawa, K.; Watanabe, J.; Takezoe, H. *Angew. Chem., Int. Ed.* **2006**, *45*, 1382.
(22) Jákli, A.; Nair, G. G.; Lee, C. K.; Sun, R.; Chien, L. C. *Phys. Rev. E* **2001**, *63*, No. 061710.
(23) Matsumoto, E. A.; Alexander, G. P.; Kamien, R. D. *Phys. Rev. Lett.* **2009**, *103*, No. 257804.
(24) Kamien, R. D. *Rev. Mod. Phys.* **2002**, *74*, 953.
(25) Takekoshi, K.; Ema, K.; Yao, H.; Takanishi, Y.; Watanabe, J.; Takezoe, H. *Phys. Rev. Lett.* **2006**, *97*, No. 197801.
(26) The angular dependence of the birefringence was first reported by: Rastegar, A.; Wulterkens, G.; Verscharen, H.; Rasing, Th.; Heppke, G. *Rev. Sci. Instrum.* **2000**, *71*, 4492.